Particle production in Au + Au collisions at $\sqrt{s_{NN}} = 11.5\text{–}200$ GeV using the HYDJET++ framework

Gauri Devi [1,*] Satya Ranjan Nayak, [1,†] and B. K. Singh [1,2,‡]
[1] *Department of Physics, Institute of Science, Banaras Hindu University (BHU), Varanasi 221005, India*
[2] *Discipline of Natural Sciences, PDPM Indian Institute of Information Technology, Design & Manufacturing, Jabalpur 482005, India*

(Received 22 August 2025; revised 15 June 2026; accepted 9 July 2026; published 27 July 2026)

Using the HYDJET++ model, we study the production of multistrange particles (ϕ and Ω) in Au + Au collisions at $\sqrt{s_{NN}} = 11.5$, 19.6, 27, 39, and 200 GeV as functions of transverse momentum and centrality. The model calculations employ earlier freeze-out hypersurfaces for multistrange particle production and are compared with STAR experimental data. Results indicate that the ++ model demonstrates a better agreement with experimental data for multistrange particles at higher energies, particularly in relation to early thermal freeze-out. Meanwhile, the default version performs more accurately for lighter, nonstrange particles at the same energy scales. We also analyze identified particle and mixed particle ratios, providing insights into strangeness enhancement. The results provide additional constraints on parton energy loss models, contributing to a more precise determination of the transport properties of hot and dense QCD matter.

DOI: 10.1103/5x7p-qk2l

I. INTRODUCTION

In high-energy relativistic nuclear collisions, extreme temperatures (150–170 MeV) and energy densities (1–5 GeV/fm^3) are achieved [1], which leads to the formation of a free state of quarks and gluons known as the quark-gluon plasma (QGP). As the system expands and cools, it transitions back into hadronic matter, during which a large number of secondary particles are produced. By analyzing these particles, deeper insights into the thermodynamic properties of the system, like temperature, entropy density, energy density, and particle multiplicity can be obtained [1]. Particularly, at lower collision energies, these observables show distinctive changes that reflect the system's inability to sustain QGP formation and reveal important information about the QCD phase diagram and the onset of deconfinement [2]. The QCD phase diagram is typically represented as a temperature graph (T) against baryon chemical potential (μ_B). μ_B plays an important role, reflecting the abundance of baryons over antibaryons and serving as a crucial statistical thermodynamic parameter controlling the net baryon density of the hadronic fireball system. A thermalized system of different T and μ_B can be created in heavy-ion collisions by adjusting the collision energy ($\sqrt{s_{NN}}$) [2–7].

The BNL Relativistic Heavy Ion Collider (RHIC) implemented an experimental initiative called Beam Energy Scan (BES) to study the production and evolution of QGP at different beam energies and explore different phases of QGP [2,3,7]. In such an experiment, the energy dependence of p_T spectra and ratios are crucial to understand the QGP formation [2]. The particle spectra provide significant information about the system's temperature and collective flow, reflecting the dynamics of kinetic freeze-out. The Solenoidal Tracker at RHIC (STAR) [8,9] and the Pioneering High Energy Nuclear Interaction eXperiment (PHENIX) [10,11] at the RHIC experiments are designed to investigate relativistic nuclear collisions using a broad range of probes, with a particular emphasis on particles produced during the early stages of the collision, especially (multi)strange hadrons [8,9].

In $p + p$ collisions [11] hard-scattered partons fragment into jets of hadrons; these fragments are the primary source of hadrons, typically above $\geqslant 2\,\text{GeV}/c$. These $p + p$ collisions serve as a crucial baseline for understanding nuclear effects and strangeness enhancement in heavy-ion ($A + A$) collisions [11].

Among the various messengers, strange hadrons, particularly the ϕ meson, serve as an excellent messenger for exploring the QCD phase boundary and identifying the onset of deconfinement and critical phase conditions. It has two important features: first, these productions and decay resonances are affected by the Okubo-Zweig-Iizuka (OZI) rule [4,12]. This rule strongly suppresses ϕ-meson decay via three pions ($\phi \to \pi^+ + \pi^- + \pi^0$) while it does not suppress decay via two kaons ($\phi \to K^+ + K^-$ or $\phi \to K_L^0 + K_S^0$). Kaon decay gives a significant contribution (i.e., through the first decay process, 49%, and the second decay process,

*Contact author: gauri.devi13@bhu.ac.in; gauri1995devi@gmail.com
†Contact author: satyanayak@bhu.ac.in
‡Contact author: bksingh@bhu.ac.in, director@iiitdmj.ac.in

TABLE I. Centrality-dependent values of the number of participants ($\langle N_{\text{part}}\rangle$) and the number of binary collisions ($\langle N_{\text{coll}}\rangle$), using HYDJET++ simulations for Au + Au collisions at $\sqrt{s_{NN}} = 11.5-200$GeV.

Energies (GeV)	11.5		19.6		27		39		200	
Centrality (%)	$\langle N_{\text{part}}\rangle$	$\langle N_{\text{coll}}\rangle$	$\langle N_{\text{part}}\rangle$	$\langle N_{\text{coll}}\rangle$	$\langle N_{\text{part}}\rangle$	$\langle N_{\text{coll}}\rangle$	$\langle N_{\text{part}}\rangle$	$\langle N_{\text{coll}}\rangle$	$\langle N_{\text{part}}\rangle$	$\langle N_{\text{coll}}\rangle$
0–10	306.7	669.3	307.4	683.4	308.5	700.6	310	726.3	346.3	1006
10–20	212.8	420.5	213.6	429.3	214.7	440.2	216.1	456.1	223.9	562.9
20–30	145.4	257.8	146.2	263.4	147.0	269.8	148.2	279.6	155.1	345.1
30–40	95.20	148.6	95.80	151.8	96.51	155.6	97.50	161.3	103.3	199.1
40–60	46.35	59.27	46.84	60.70	47.28	62.18	47.96	64.49		
60–80	12.05	11.08	12.20	11.32	12.37	11.60	12.63	12.03	14.25	14.97

34%) in ϕ-meson decay, pion decay gives no significant contribution (i.e., 8%) in ϕ-meson decay, and other decay is not substantial. Second, their cross section is small for scattering with nonstrange hadrons during the hadronic phase [4,12].

In previous studies [13–16], the HYDJET++ model has been successfully utilized to describe strange-particle production in the high-temperature and low-baryon chemical potential regime, corresponding to ultrarelativistic collision energies. Now, we are exploring the low-temperature and high-baryon chemical potential regime, corresponding to lower collision energies by using the HYDJET++ model. This exploration provides new insights into the energy dependence of particle production, strangeness enhancement, and the QCD critical point through transverse momentum (p_T) spectra, average transverse momentum ($\langle p_T\rangle$), p_T-spectra ratios with respect to the system's energies, and baryon-to-meson and multistrange to single-strange hadron ratios.

The outline of this study is as follows. Section II provides a brief description of the HYDJET + +model [13,15–24]. Section III A highlights the difference between the thermal freeze-out T_{th} used in HYDJET++ and T_{th}'s extracted using other methods like Tsallis, blast-wave, and exponential fits. Section III B highlights the precise measurements of the p_T spectra and average $\langle p_T\rangle$ for ϕ and Ω hadrons. These results are compared to the available STAR experiment data [9,25–27], focusing on collisions at beam scan RHIC energies [25]. Section III C discusses the particle ratios in the RHIC Beam Energy Scan, while Sec. IV provides a summary of our main findings.

II. BRIEF INTRODUCTION TO THE HYDJET++ MODEL

The HYDJET++ model combines the soft and hard components' particle production, simultaneously allowing the study of the dynamics of relativistic heavy-ion collisions [20,22]. The soft component in HYDJET++ denotes a thermalized hadronic state, simulated through the multiparticle hadron production using a fast Monte Carlo (MC) generator [23,24]. This generator uses a parametrized relativistic hydrodynamics model that considers the chemical (T_{ch}) and thermal (T_{th}) freeze-out hypersurfaces to explain the system's evolution. At chemical freeze-out, hadrons are considered to be in chemical equilibrium, which determines the final particle composition. At thermal freeze-out, local thermal equilibrium is considered, which determines the momentum distributions of hadrons [28].

This stage involves statistical particle production from the grand-canonical ensemble that incorporates thermodynamic parameters such as T, μ, and system volume (V) and simultaneously includes treatment of collective flow effects to account for the medium's expansion. Here, the model assumes longitudinal boost invariance and incorporates transverse radial flow, quantified by the maximum transverse flow rapidity (ρ_u^{max}) [21]. These flow effects significantly influence the shape of transverse momentum (p_T) spectra, especially for heavier particles, which receive a stronger boost during the medium's expansion.

On the other hand, the hard component in HYDJET++ involves generating multijets using a binomial distribution inside the PYQUEN energy loss model [22]. The PYQUEN model for single hard nucleon-nucleon subcollisions was developed as a modification of jet events produced by the PYTHIA_6.4 [29] generator for hadron-hadron interactions [20]. Following this, the final hadronization of hard partons takes place according to the Lund string model [20]. The average number of jets produced in an *AA* collision is determined by multiplying the binary *NN* collisions at a given impact parameter with the integral cross section of the hard process in *NN* collisions with a minimum transverse momentum transfer (p_T^{min}). The p_T^{min} serves as the threshold separating soft particle emission from hard scatterings associated with jet formation effects [2,22].

The production of heavier hadrons (such as strange and multistrange baryons) is more sensitive to the freeze-out temperature due to their larger mass, requiring higher thermal energy for their creation. In contrast, lighter hadrons (such as pions) are more abundantly produced even at lower temperatures. Thus, the relative abundances and spectra of different particle species carry imprints of the system's temperature and evolution.

This version of HYDJET++ is an extended adaptation of the previous HYDJET++ implementation at energies available at the RHIC and the CERN Large Hadron Collider [13,18], now tailored for Beam Energy Scan at energies available at the RHIC. We have modified hadron-species-dependent freeze-out parameters like T_{th}, T_{ch}, and a phase-space occupancy factor, γ_s [30], in the default HYDJET++ framework. These parameters were extracted by comparing the p_T- spectra of charged yields from modified model to experimental data [2] and as also mentioned in Ref. [18]. The

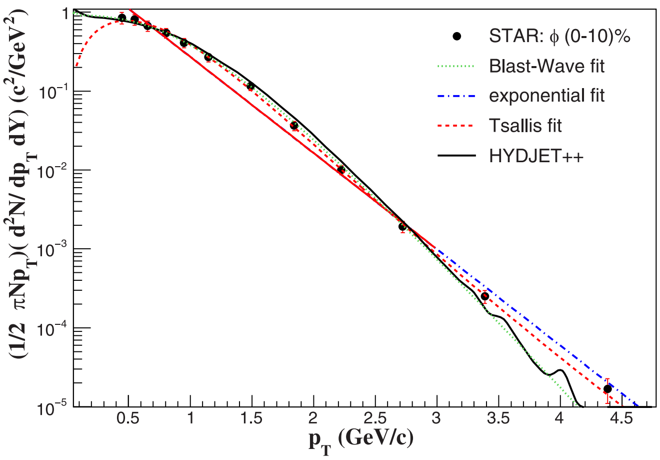

FIG. 1. The p_T spectra of ϕ mesons using Tsallis distribution fit, blast-wave fit, exponential fit, and HYDJET++ for central collisions of Au + Au collisions at $\sqrt{s_{NN}} = 39$ GeV. The markers denote the STAR experimental data [9], while the lines correspond to the results obtained from different methods.

last parameter γ_s has been adjusted as a centrality-dependent variable [25], as detailed in Sec. III. γ_s is introduced to account for the potential nonequilibrium of strange quarks.

The geometrical parameters in HYDJET++, calculated using the two-parameter Fermi (2-pF) form Monte Carlo–Glauber model, show consistency with the experimental data reported by the STAR Collaboration [2], where the number of participating collisions ($\langle N_{\text{part}}\rangle$) and the number of binary collisions ($\langle N_{\text{coll}}\rangle$) are also obtained from Glauber calculations. In Table I, we present the correlation between $\langle N_{\text{coll}}\rangle$ and $\langle N_{\text{part}}\rangle$ across various centrality classes (%), as obtained from the geometrical output of the HYDJET++ model. Furthermore, by comparing the p_T spectra to experimental data [2], we have adopted the same values of chemical parameters (γ_s, μ_B, T_{ch}) and the thermal parameter (T_{th}) for RHIC beam scan energies at 11.5, 19.6, 27, and 39 GeV from the STAR experiment [2] and optimized all the same parameters for RHIC beam energy at 200 GeV from Ref. [18]. In the STAR experiment, these parameters were typically extracted through statistical thermal model analyses with the thermus package [31], using either the grand-canonical ensemble (GCE) or the strangeness canonical ensemble (SCE). While the GCE is suitable at higher energies with abundant strangeness, the SCE is required at lower energies with limited strangeness production. In this work we adopt the GCE approach parameters, as the RHIC BES program spans a broad energy range.

III. RESULTS AND DISCUSSIONS

A. Freeze-out temperatures

The thermal freeze-out hypersurface determines the soft hadroproduction in HYDJET++; it is necessary to understand the difference between T_{th} used in HYDJET++ and T_{th}'s extracted using other methods. One of the popular ways

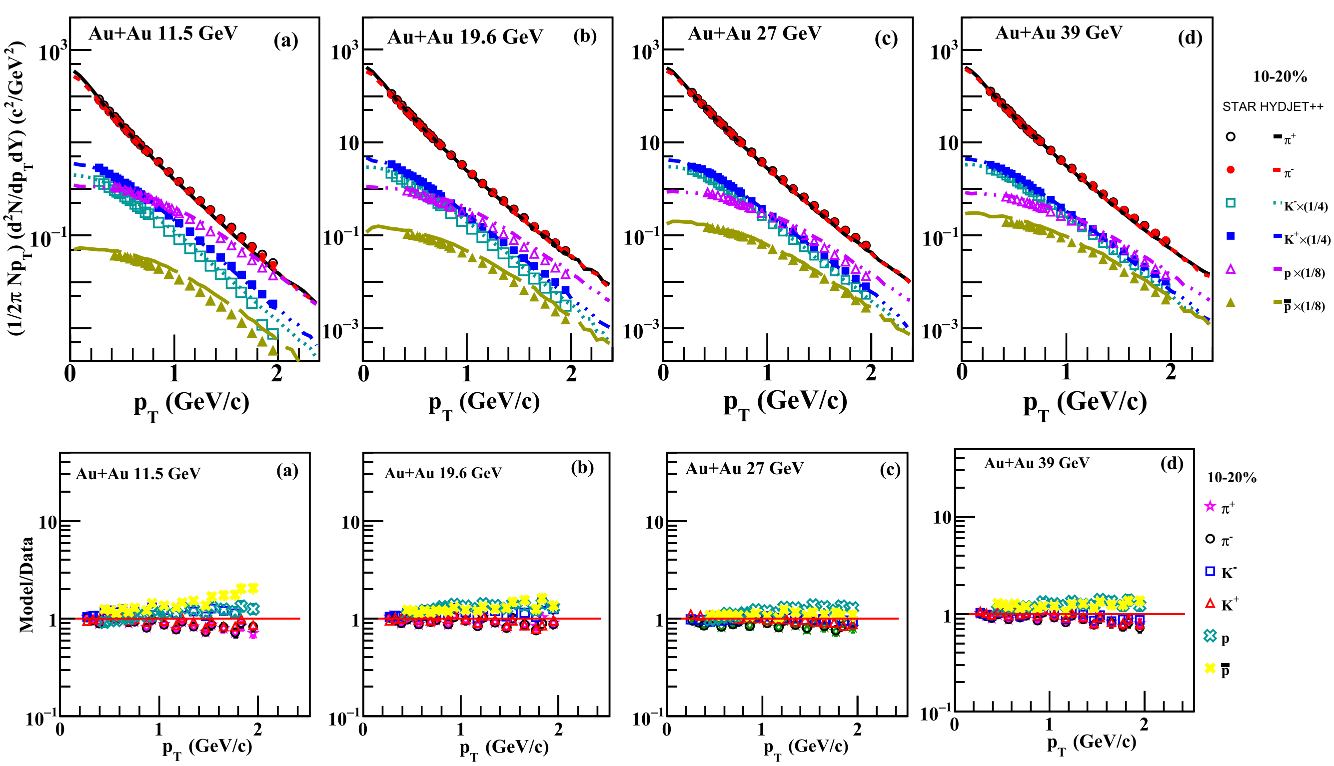

FIG. 2. Upper panels: The p_T spectra of primary charged particles as a function of p_T in Au + Au collisions at $\sqrt{s_{NN}} = 11.5$–200 GeV. The lines represent HYDJET++ results while the markers represent STAR experimental data [9,25,27]. Lower panels: Ratios of model predictions to experimental data for corresponding charged particles.

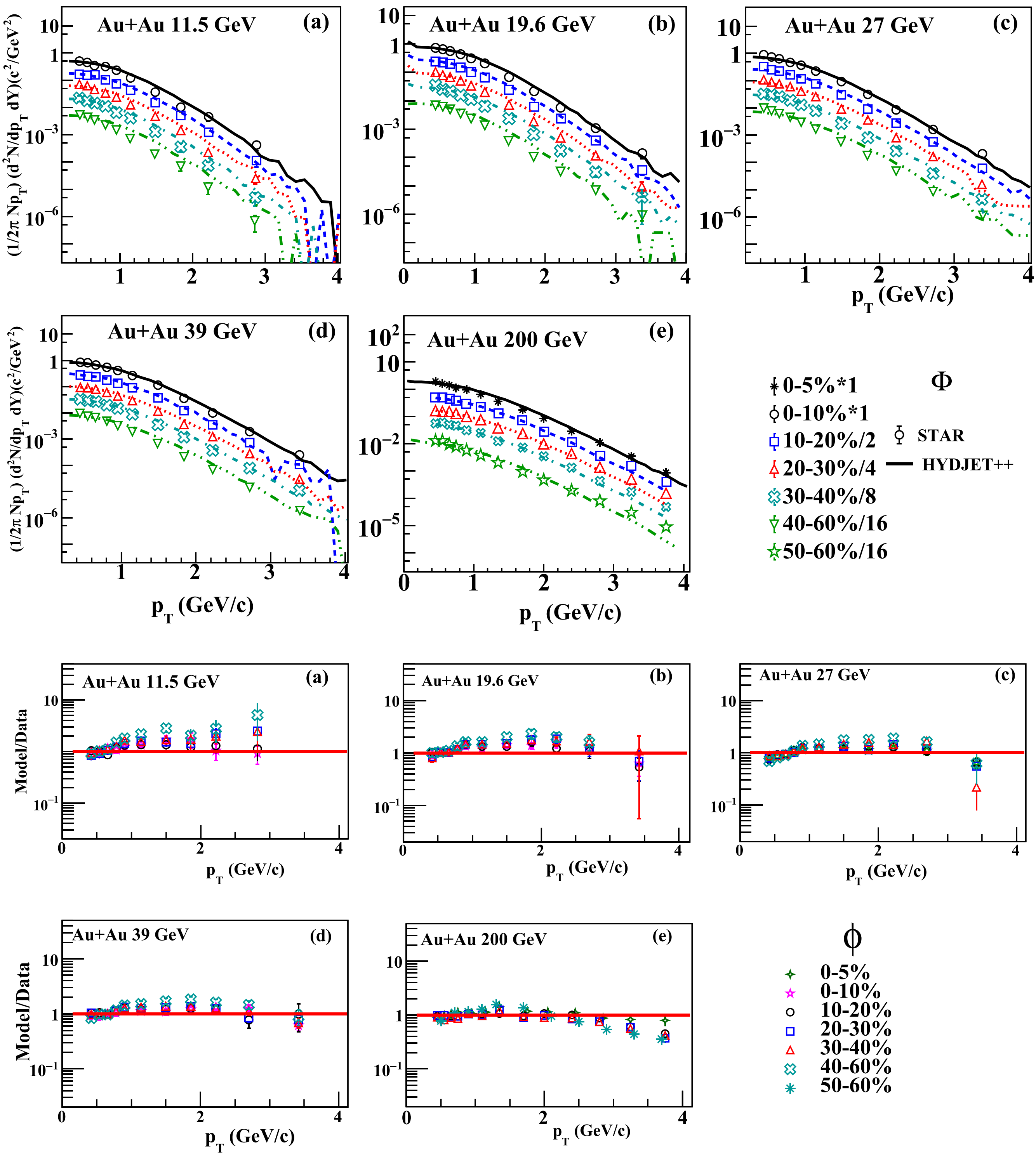

FIG. 3. Upper panels: The p_T spectra of ϕ-mesons as a function of p_T in Au + Au collisions at $\sqrt{s_{NN}} = 11.5$–200 GeV. The lines represent HYDJET++ results while the markers represent STAR experimental data [9,25,27]. Lower panels: Ratios of model predictions to experimental data for ϕ mesons.

to extract $T_{\rm th}$ is to fit the data with a distribution like Tsallis or by the blast-wave fit. A typical Tsallis distribution is given by [32]

$$\frac{d^2N}{2\pi\, p_T\, dp_T\, dy} = g v m_T \frac{\cosh y}{(2\pi)^3}[1-(q-1)(m_T \cosh y - \mu)/T],$$

where g is the degeneracy, v is the volume, T is same as $T_{\rm th}$, and the nonextensive parameter q refers to the system's deviation from thermalization (at $q = 1$ it becomes Boltzmann's distribution). It was reported in a previous study that the value of q increases with increasing beam energy, which is

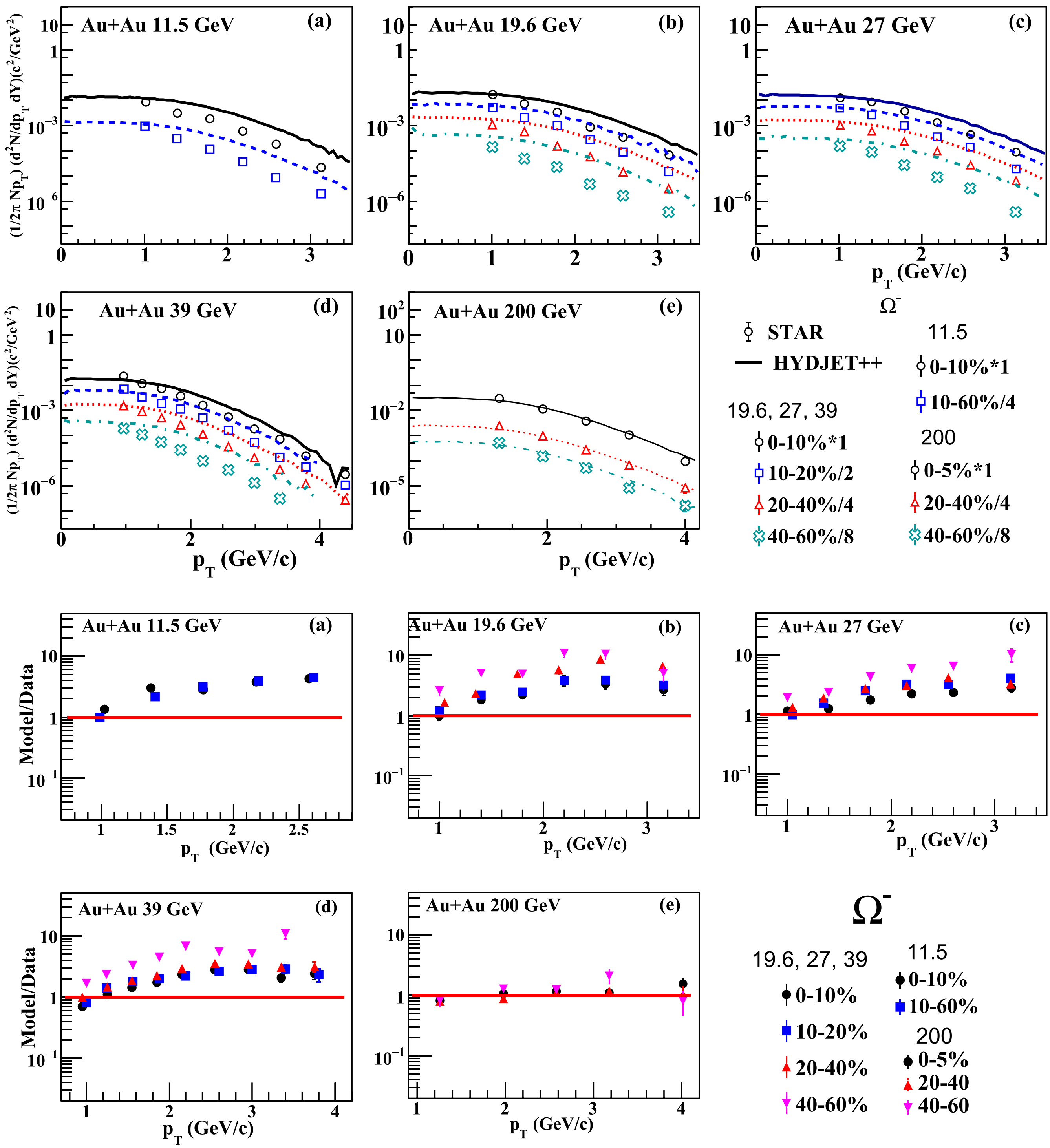

FIG. 4. Upper panels: The p_T spectra of Ω^- baryons as a function of p_T in Au + Au collisions at $\sqrt{s_{NN}} = 11.5$–200 GeV. The lines represent HYDJET++ results while the markers represent STAR experimental data [9,26,27]. Lower panels: Ratios of model predictions to experimental data for Ω^- baryons.

concerning as the systems formed at high $\sqrt{s_{NN}}$ are known to thermalize due to high temperature and longer lifetime of the QGP [32]. We have fitted the transverse momentum distribution of ϕ mesons using the Tsallis distribution in Fig. 1. The resulting value of T was 184 MeV, much higher than the T_{th} value used in this work. This difference arises as HYDJET++ assumes a fully thermal system while the Tsallis distribution assumes a near-equilibrated system. In this work, we have matched the p_T data by simultaneously tuning the thermal freeze-out temperature T_{th} and the maximum transverse flow rapidity ρ_{max}. These parameters are similar to the ones used in the blast-wave fit. However, a key difference between these

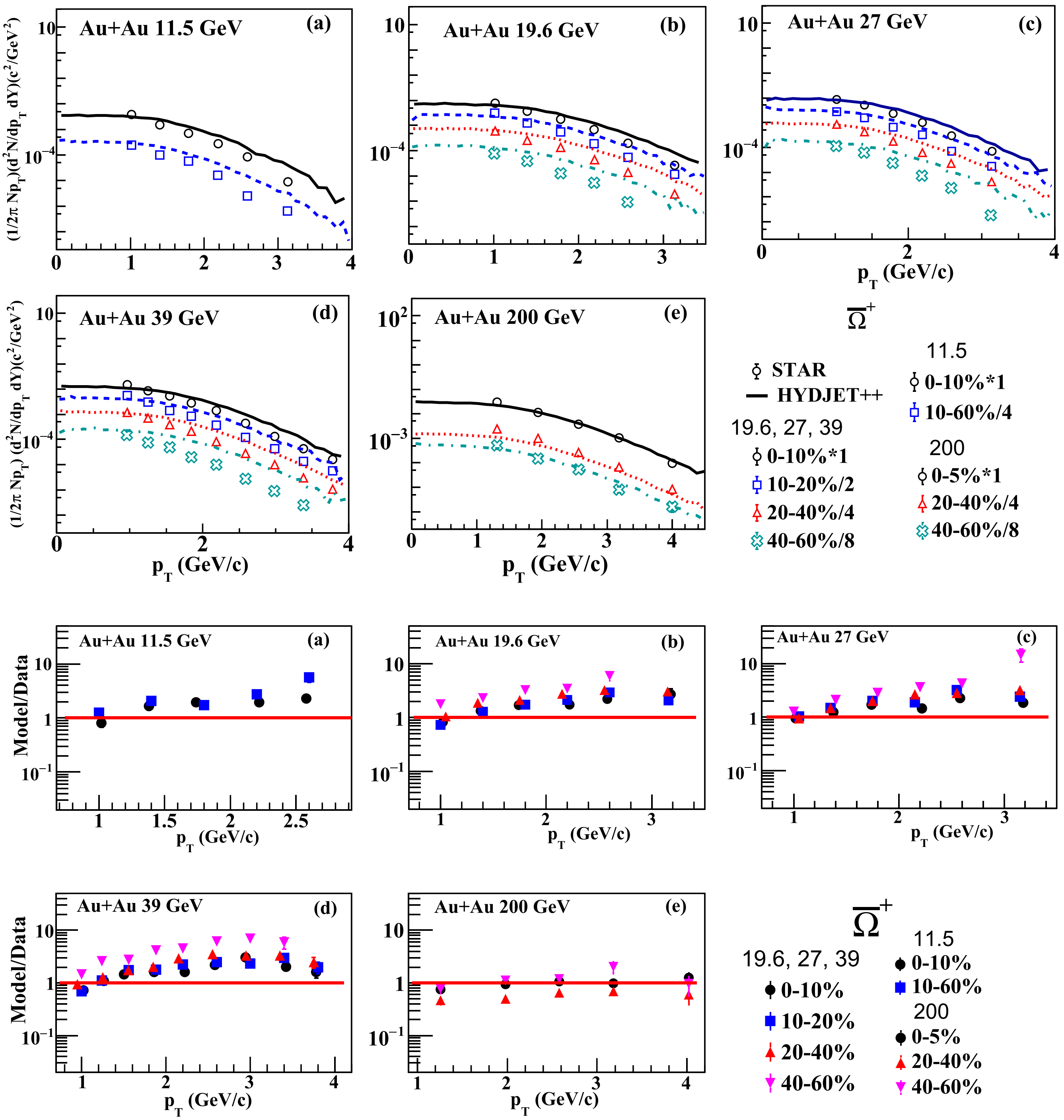

FIG. 5. Upper panels: p_T spectra of $\overline{\Omega}^+$ baryons from Au + Au collisions at $\sqrt{s_{NN}}$ = 11.5–200 GeV. The lines represent HYDJET++ results while the markers represent STAR experimental data [9,26,27]. Lower panels: Ratios of model predictions-to-experimental data for $\overline{\Omega}^+$ baryons.

two is that HYDJET++ is a Monte Carlo event generator rather than a fitting tool. Unlike the blast-wave model [33], the HYDJET++ simulations include contributions from jets and resonance decays, which affect the p_T spectra and the choice of the T_{th} parameter. Hence, the T_{th} values used in this work are different than the ones extracted from the blast-wave fit from the corresponding paper [2].

B. Transverse momentum spectra (p_T) and mean p_T ($\langle p_T \rangle$)

From Fig. 2, the p_T spectra exhibit the expected inverse slope hierarchy ($\pi < K < p$). The yields of charged pions, kaons, and antiprotons decrease with decreasing collision energy, whereas the proton yield is highest at 11.5 GeV, indicating the largest baryon density (baryon chemical potential) at midrapidity at this energy, consistent with both

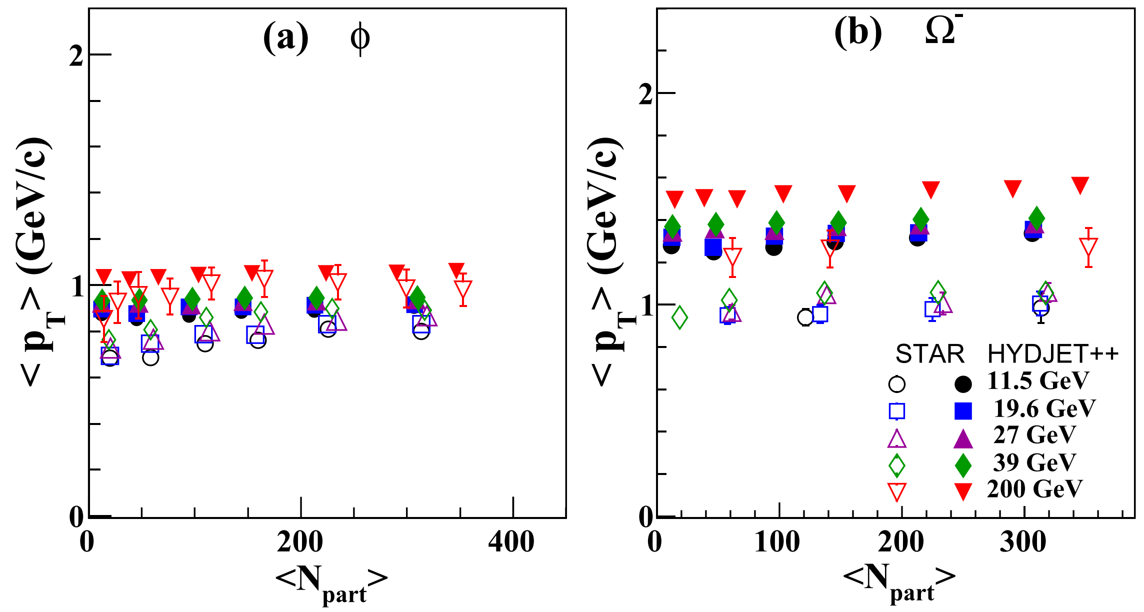

FIG. 6. $\langle p_T \rangle$ as a function of $\langle N_{\text{part}} \rangle$ in Au + Au collisions at $\sqrt{s_{NN}} = 11.5-200$ GeV. The solid markers represent HYDJET++ results while the open markers represent STAR experimental data [9,36].

experimental data [2] and our framework. A recent HYDJET++ study by Nayak *et al.* [34] has addressed light charged particle production at RHIC BES energies. In this work, we provide a systematic description within the same framework, showing that the HYDJET++ baseline reasonably reproduces the overall spectral shapes and magnitudes, thereby establishing a reliable basis for the study of multistrange particle production. The transverse momentum spectra of the multistrange particles are significant observables, since they provide essential information about the equilibrium dynamics and isotropy of the system in high-energy collisions. These calculations give the information that the production of ϕ and Ω supports the fact that jet production is suppressed in events where one or more strange particles are produced [13,16].

Figures 3–5 present the transverse momentum spectra of the ϕ mesons and Ω baryons obtained in comparison with the STAR experimental data [9,25–27]. The solid line represents a constant fit applied to the model-to-data ratio. The figures also present the model-to-data ratios, which indicate the level of agreement between the HYDJET++ predictions and the experimental results. The HYDJET++ calculations describe the data well in the central collision at energies higher than those of the peripheral collisions and lower energies. Figures 4 and 5 show more deviation of the model-to-data ratios from unity towards peripheral events. The uncertainty is higher for Ω baryons than the ϕ mesons, which strongly supports the flavor-dependence particle production at lower energies. These spectra also reveal a significant difference in the invariant yield values for particles and the corresponding antiparticles [35]. This difference increases with decreasing energy ($\sqrt{s_{NN}}$) (or increasing μ_B) and is larger for the baryons. This also implies that particles and antiparticles are no longer consistent with the matter-antimatter symmetry towards lower energy that was observed at $\sqrt{s_{NN}} = 200$ GeV [35].

Figure 6 presents the mean $\langle p_T \rangle$ of both particles at RHIC BES energies and the available experimental results [9,36]. Figure 6(a) presents that the results of the particles ϕ at RHIC BES energies match well within the uncertainty range for central collisions and higher energies. In contrast, Figure 6(b) shows that the HYDJET++ predictions for Ω baryons at RHIC BES energies overpredict the experimental data across all collision centralities and energies. This discrepancy indicates limitations of the HYDJET++ framework in describing baryon production in the RHIC BES energy regime. The freeze-out conditions appear to be more accurately tuned for mesons like ϕ than for baryons like Ω, leading to the observed discrepancies. Additionally, the model is also less sensitive to certain mechanisms, such as baryon coalescence which carries more weight for multistrange baryons like Ω [18,37].

C. Particle ratio

Figures 7–10 present the particle yield ratios (in terms of energy ratios) and different particle ratios, $N[\Omega^-(\overline{\Omega}^+)]/[N(\phi)]$, $N(\overline{\Omega}^+)/N(\Omega^-)$, $N[\phi(\Omega^-)]/N(K^-)$, and $N(\Omega^- + \overline{\Omega}^+)/[2N(\phi)]$, as a function of p_T and compare them with the available experimental data [27,38] for most central collisions from Au + Au collisions at $\sqrt{s_{NN}} = 11.5$–200 GeV. Figure 7 presents the particle yield ratios at 19.6, 27, 39, and 200 GeV to 11.5 GeV and shows a suppression of particle production with flavor towards high- to low-energy systems while showing an enhancement of particle production as a function of p_T. Figure 8 presents the baryon-to-meson $[N(\Omega^-)/N(K^-)]$ and meson-to-meson $[N(\phi)/N(K^-)]$ ratios. These results show different shapes of particle p_T distributions at low and intermediate p_T in central collisions, which indicates that the number of quarks is the main factor and baryons are suppressed more than mesons. Expanding on this,

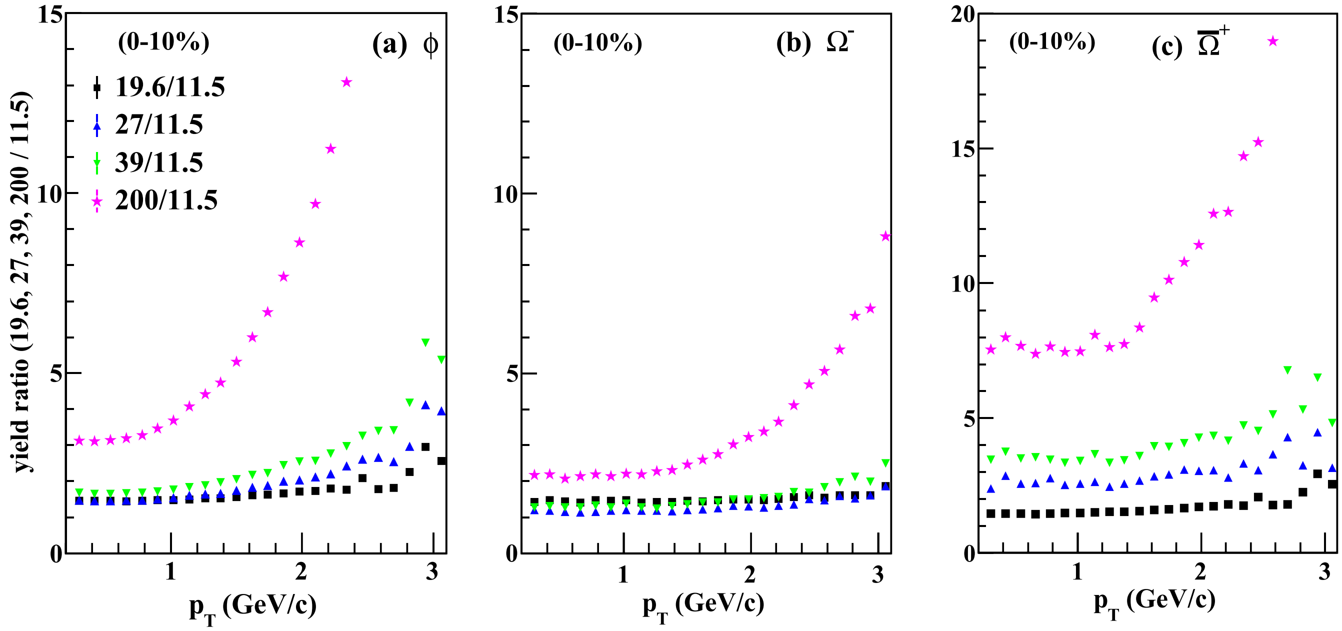

FIG. 7. Particle yield ratios (in term of energy ratios) as a function of p_T in Au + Au collisions at $\sqrt{s_{NN}} = 11.5$–200 GeV. The solid markers represent HYDJET++ results.

Fig. 9 shows that the $N(\Omega^- + \overline{\Omega}^+)/[N(\phi)]$ ratios in central (0–10%) Au + Au collisions at $\sqrt{s_{NN}} = 11.5$–200 GeV exhibit a consistent qualitative increase with p_T displaying an approximately linear trend similar to the STAR experiment results [27]. However, the model systematically overpredicts the experimental values, particularly at lower collision energies. This overprediction may arise from the model's treatment of strangeness enhancement, where the parametrization of strange quark production in the soft component may not adequately reflect the reduced partonic collectivity and incomplete thermalization at lower energy. Furthermore, Fig. 10 presents the ratio of antiparticle to particle ($\overline{B}/B$) at $\sqrt{s_{NN}} = 11.5$–200 GeV. A variation with energy supports that the matter-antimatter symmetry does not hold at lower energies. At lower energies, the ratio tends to be less than 1, which supports the notion that antiparticle production is less than particle production. This trend is consistent with experimental results for the RHIC beam scan energy [9]. This property of antiparticle/particle ratios is qualitatively well described in the statistical model [34,39].

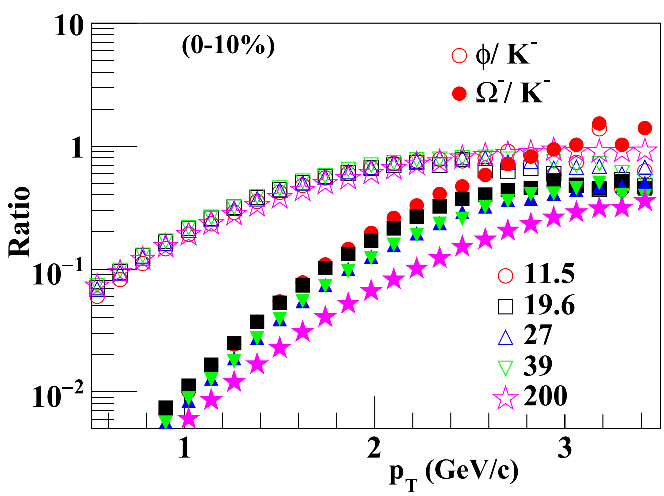

FIG. 8. Particle ratios $N(\phi)/N(K^-)$ (represents by open markers) and $N(\Omega^-)/N(K^-)$ (represents by solid markers) as a function of p_T in Au + Au collisions at $\sqrt{s_{NN}} = 11.5$–200 GeV.

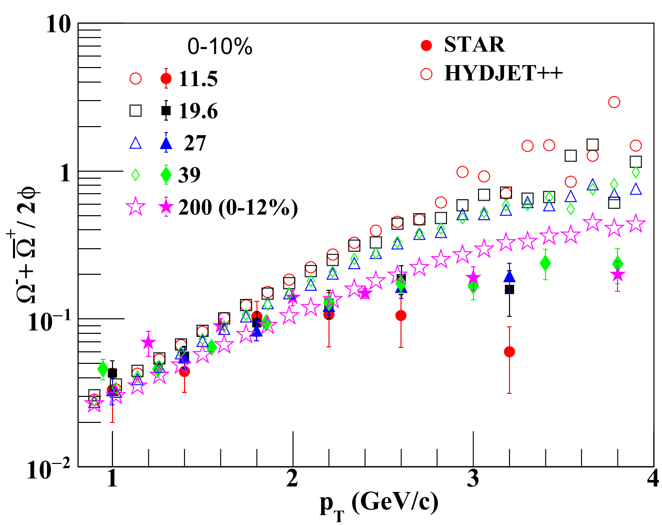

FIG. 9. Baryon-to-meson ratio $N(\Omega^- + \overline{\Omega}^+)/[2N(\phi)]$ as a function of p_T in Au + Au collisions at $\sqrt{s_{NN}} = 11.5$–200 GeV. The open markers represent HYDJET++ results and the solid markers represent STAR experimental data [27].

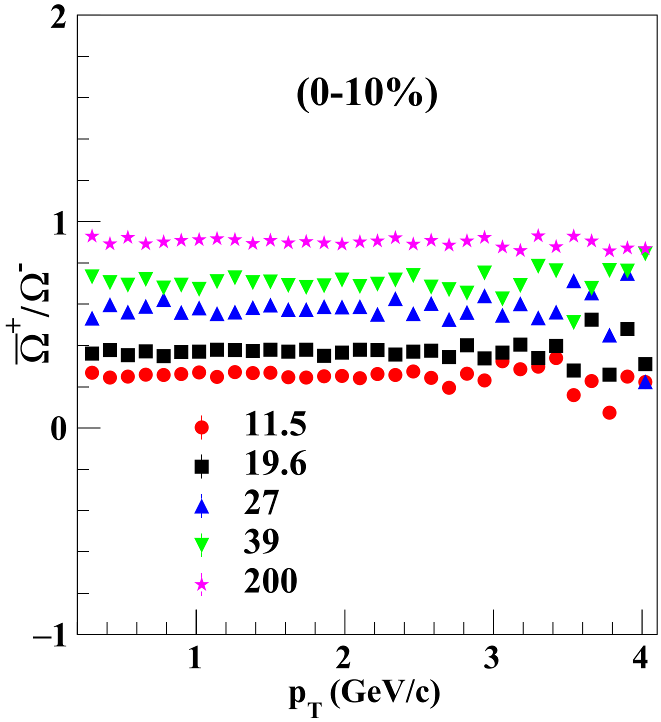

FIG. 10. Antiparticle-to-particle ratio $N(\overline{\Omega}^+)/N(\Omega^-)$ as a function of p_T in Au + Au collisions at $\sqrt{s_{NN}} = 11.5$–200 GeV. The solid markers represent HYDJET++ results.

IV. CONCLUSION

In conclusion, our study demonstrates that the simulated bulk properties using the HYDJET++ model are sensitive to the choice of input parameters. Details of the analysis method for ϕ mesons and Ω baryons are presented. This study demonstates the dependence of multistrange particle production on energy, $\langle N_{\text{part}}\rangle$, and $\langle N_{\text{coll}}\rangle$, and reports the differences in freeze-out temperatures between HYDJET++ and other thermal extraction methods. Additionally, results on p_T spectra, $\langle p_T\rangle$, particle yield ratios (relative to 11.5 GeV energies) as a function of p_T, and particle ratios for five collision systems are presented. By comparing the model predictions with the experimental data, we assess the model performance in describing the multistrange particle production mechanism at RHIC Beam Energy Scan. The transverse momentum (p_T) spectra illustrate a clear hardening with increasing collision energy, and noticeable deviations are observed for the ϕ and Ω particles, especially at lower collision energies. This behavior may be due to the stronger collective flow at higher energies. At the same time, these discrepancies suggest certain limitations of the current model implementation in describing multistrange particle production over the full energy range. The increasing discrepancy at lower $\sqrt{s_{NN}}$ may be attributed to several factors. First, the reduced parton energy loss at lower energies can weaken the jet-medium interaction effects incorporated in the model. Second, the assumption of boost invariance used in the HYDJET++ framework may become less valid in the low-energy regime, where longitudinal dynamics are more complex. Third, stronger baryon chemical potential effects at low $\sqrt{s_{NN}}$ can influence the production of strange and multistrange hadrons in ways that are not fully captured by the model. Therefore, the present results should be interpreted as providing a qualitative description of the observed trends rather than a complete understanding of the multistrange particle production mechanism across all collision energies. It also suggests ϕ achieves the thermal resonance equilibrium while Ω does not achieve equilibrium due to heavier mass with less hadronic interaction. Additionally, in calculations of particle yield ratios (relative to 11.5-GeV energies) of multistrange hadrons at low to intermediate p_T in central collisions, we have found a stronger dependence of the p_T shape in ϕ and $\overline{\Omega}^+$ than in Ω^- towards 19.6/11.5 to 200/11.5 energy ratios. Following this, the baryon-to-meson and meson-to-meson ratios show the suppression of strange-quark production in 11.5 GeV compared to $\sqrt{s_{NN}} = 19.6$ GeV. These features suggest that there is likely a change in the underlying strange-quark dynamics in the bulk QCD matter responsible for Ω and ϕ production. Our measurements point to collision energies below 19.6 GeV for further investigation of a possible transition from partonic dominant matter ($\sqrt{s_{NN}} > 19.6$ GeV) to hadronic dominant matter ($\sqrt{s_{NN}} < 11.5$ GeV). We also see that the ratios are closer to the value of one towards 200 GeV, reflecting the approach to baryon-antibaryon symmetry at midrapidity as the collision energy increases. Furthermore, by analyzing the p_T spectra and particle ratio patterns across various beam energies, we can provide more comprehensive insights into the evolution of the QGP medium and the mechanisms governing multistrange particle production in heavy-ion collisions. These findings not only enhance our understanding of strangeness dynamics in a baryon-rich QCD region but also serve as a valuable reference for selecting optimal model parameters in future beam-energy-dependent studies.

ACKNOWLEDGMENTS

B.K.S. gratefully acknowledges the financial support provided by the BHU Institutions of Eminence (IoE) under Grant No. 6031, Government of India. G.D. and S.R.N. are thankful for the support of non-net fellowships under the central university scheme.

DATA AVAILABILITY

The data that support the findings of this article are not publicly available. The data are available from the authors upon reasonable request.

[1] K. Adcox *et al.* (PHENIX Collaboration), Formation of dense partonic matter in relativistic nucleus–nucleus collisions at RHIC: Experimental evaluation by the PHENIX Collaboration, Nucl. Phys. A **757**, 184 (2005).

[2] L. Adamczyk *et al.* (STAR Collaboration), Bulk properties of the medium produced in relativistic heavy-ion collisions from the beam energy scan program, Phys. Rev. C **96**, 044904 (2017).

[3] B. I. Abelev *et al.* (STAR Collaboration), Energy and system size dependence of ϕ meson production in Cu + Cu and Au + Au collisions, Phys. Lett. B **673**, 183 (2009).
[4] A. Shor, φ-meson production as a probe of the quark-gluon plasma, Phys. Rev. Lett. **54**, 1122 (1985).
[5] C. P. Singh, V. K. Tiwari, and K. K. Singh, Production of φ as a potential probe for QGP formation, Phys. Lett. B **393**, 188 (1997).
[6] C. P. Singh, Comment on "φ-meson production as a probe of the quark-gluon plasma", Phys. Rev. Lett. **56**, 1750 (1986).
[7] Y. J. Ye, J. H. Chen, Y. G. Ma, S. Zhang, and C. Zhong, Ω and ϕ in Au + Au collisions at $\sqrt{s_{\rm NN}} = 200$ and 11.5 GeV from a multiphase transport model, Chin. Phys. C **41**, 084101 (2017).
[8] M. Abdallah *et al.* (STAR Collaboration), Azimuthal anisotropy measurement of (multi)strange hadrons in Au + Au collisions at $\sqrt{s_{\rm NN}} = 54.4$ GeV, Phys. Rev. C **107**, 024912 (2023).
[9] J. Adam *et al.* (STAR Collaboration), Strange hadron production in Au + Au collisions at $\sqrt{s_{NN}} = 7.7$, 11.5, 19.6, 27, and 39 GeV, Phys. Rev. C **102**, 034909 (2020).
[10] A. Adare *et al.* (PHENIX Collaboration), Spectra and ratios of identified particles in Au + Au and d + Au collisions at $\sqrt{s_{NN}} = 200$ GeV, Phys. Rev. C **88**, 024906 (2013).
[11] A. Adare *et al.* (PHENIX Collaboration), Identified charged hadron production in $p + p$ collisions at $\sqrt{s} = 200$ and 62.4 GeV, Phys. Rev. C **83**, 064903 (2011).
[12] S. Okubo, φ-meson and unitary symmetry model, Phys. Lett. **5**, 165 (1963).
[13] G. Devi and B. K. Singh, Production of multistrange hadrons in Pb + Pb collisions at energies available at the CERN Large Hadron Collider using the HYDJET++ model, Phys. Rev. C **112**, 034907 (2025).
[14] G. Devi, A. Singh, and B. K. Singh, pT-spectra and elliptic flow of Φ meson in Au + Au collisions at RHIC energies using HYDJET++ model; DAE Symp, Nucl. Phys. **67**, 1059 (2024).
[15] G. Devi, A. Singh, S. Pandey, and B. K. Singh, Higher flow harmonics of strange hadrons in Au + Au collisions at $\sqrt{s_{\rm NN}} =$ 200 GeV and Pb + Pb collisions at $\sqrt{s_{\rm NN}} = 2.76$ TeV with HYDJET++ model, Eur. Phys. J. Plus **138**, 921 (2023).
[16] A. Singh, P. K. Srivastava, G. Devi, and B. K. Singh, Production and enhancement of (multi-) strange hadrons in Au + Au collisions at $\sqrt{s_{NN}} = 200$ GeV RHIC energy and Pb + Pb collisions at $\sqrt{s_{NN}} = 2.76$ TeV LHC energy, Phys. Rev. C **107**, 024906 (2023).
[17] L. V. Bravina, G. K. Eyyubova, V. L. Korotkikh, I. P. Lokhtin, S. V. Petrushanko, A. M. Snigirev, and E. E. Zabrodin, Jets and elliptic flow correlations at low and high transverse momenta in ultrarelativistic $A + A$ collisions, Phys. Rev. C **103**, 034905 (2021).
[18] G. Devi, A. Singh, and B. K. Singh, p_T-spectra, nuclear modification factors (R_{AA}, and R_{CP}) of (multi-) strange hadrons in Au+Au collisions at $\sqrt{s_{NN}} = 200$ GeV with HYDJET++, J. Phys. G: Nucl. Part. Phys. **51**, 095203 (2024).
[19] I. P. Lokhtin, A. V. Belyaev, L. V. Malinina, S. V. Petrushanko, E. P. Rogochaya, and A. M. Snigirev, Hadron spectra, flow and correlations in PbPb collisions at the LHC: Interplay between soft and hard physics, Eur. Phys. J. C **72**, 2045 (2012).
[20] I. P. Lokhtin, L. V. Malinina, S. V. Petrushanko, A. M. Snigirev, I. Arsene, and K. Tywoniuk, Modeling the jet quenching in hot and dense QCD matter, Nonlinear Phenom. Complex Syst. **12**, 348 (2009).
[21] I. P. Lokhtin, L. V. Malinina, S. V. Petrushanko, A. M. Snigirev, I. Arsene, and K. Tywoniuk, Heavy ion event generator HYDJET++ (HYDrodynamics plus JETs), Comput. Phys. Commun. **180**, 779 (2009).
[22] I. P. Lokhtin and A. M. Snigirev, A model of jet quenching in ultrarelativistic heavy ion collisions and high-$p_{\rm T}$ hadron spectra at RHIC, Eur. Phys. J. C **45**, 211 (2006).
[23] N. S. Amelin, R. Lednicky, T. A. Pocheptsov, I. P. Lokhtin, L. V. Malinina, A. M. Snigirev, I. A. Karpenko, and Y. M. Sinyukov, Fast hadron freeze-out generator, Phys. Rev. C **74**, 064901 (2006).
[24] N. S. Amelin, R. Lednicky, I. P. Lokhtin, L. V. Malinina, A. M. Snigirev, I. A. Karpenko, Y. M. Sinyukov, I. Arsene, and L. Bravina, Fast hadron freeze-out generator. II. Noncentral collisions, Phys. Rev. C **77**, 014903 (2008).
[25] B. I. Abelev *et al.* (STAR Collaboration), Measurements of ϕ meson production in relativistic heavy-ion collisions at the BNL Relativistic Heavy Ion Collider (RHIC), Phys. Rev. C **79**, 064903 (2009).
[26] J. Adams *et al.* (STAR Collaboration), Scaling properties of hyperon production in Au + Au collisions at $\sqrt{s_{NN}} = 200$ GeV, Phys. Rev. Lett. **98**, 062301 (2007).
[27] L. Adamczyk *et al.* (STAR Collaboration), Probing parton dynamics of QCD matter with Ω and ϕ production, Phys. Rev. C **93**, 021903 (2016).
[28] L. V. Bravina, I. P. Lokhtin, L. V. Malinina, S. V. Petrushanko, A. M. Snigirev, and E. E. Zabrodin, Dynamical vs geometric anisotropy in relativistic heavy-ion collisions: Which one prevails? Eur. Phys. J. A **53**, 219 (2017).
[29] T. Sjöstrand, S. Mrenna, and P. Z. Skands, PYTHIA 6.4 physics and manual, J. High Energy Phys. 05 (2006) 026.
[30] P. Castorina, S. Plumari, and H. Satz, Universal strangeness production in hadronic and nuclear collisions, Int. J. Mod. Phys. E **25**, 1650058 (2016).
[31] S. Wheaton, J. Cleymans, and M. Hauer, THERMUS—A thermal model package for ROOT, Comput. Phys. Commun. **180**, 84 (2009).
[32] J. Tao, W. Wu, M. Wang, H. Zheng, W. Zhang, L. Zhu, and A. Bonasera, The novel scaling of Tsallis parameters from the transverse momentum spectra of charged particles in heavy-ion collisions, Particles **5**, 146 (2022).
[33] E. Schnedermann, J. Sollfrank, and U. W. Heinz, Thermal phenomenology of hadrons from 200A GeV S+S collisions, Phys. Rev. C **48**, 2462 (1993).
[34] S. R. Nayak, S. Pandey, and B. K. Singh, Beam energy dependence of transverse momentum distribution and elliptic flow in Au–Au collisions using HYDJET++ model, Eur. Phys. J. Plus **140**, 375 (2025).
[35] L. Adamczyk *et al.* (STAR Collaboration), Elliptic flow of identified hadrons in Au+Au collisions at $\sqrt{s_{NN}} = 7.7$–62.4 GeV, Phys. Rev. C **88**, 014902 (2013).

[36] B. I. Abelev *et al.* (STAR Collaboration), Systematic measurements of identified particle spectra in pp, $d + \text{Au}$, and $\text{Au} + \text{Au}$ collisions at the STAR detector, Phys. Rev. C **79**, 034909 (2009).
[37] M. Waqas and G. X. Peng, Study of dependence of kinetic freezeout temperature on the production cross-section of particles in various centrality intervals in Au–Au and Pb–Pb collisions at high energies, Entropy **23**, 488 (2021).
[38] J. Aichelin and K. Werner, Is the centrality dependence of the elliptic flow v_2 and of the average $\langle p_T \rangle$ more than a core-corona effect? Phys. Rev. C **82**, 034906 (2010).
[39] J. Cleymans, I. Kraus, H. Oeschler, K. Redlich, and S. Wheaton, Statistical model predictions for particle ratios at $\sqrt{s_{NN}} = 5.5$ TeV, Phys. Rev. C **74**, 034903 (2006).